STUDY OF SPECTRAL VARIABILITY OF DIRECT AND SCATTERED SOLAR RADIATION

S.I. Dolgii, V.V. Zuev, and V.N. Marichev

Institute of Atmospheric Optics,
Siberian Branch of the Russian Academy of Sciences, Tomsk
Received December 30, 1997

A spectrophotometer for studying spectral variability of direct and scattered solar radiation is described along with the measurement and calibration techniques. Some results obtained during the measurement campaign of 1996 are presented.

An influence of cloudiness upon spectral behavior of downward flux of the short-wave solar radiation is one of significant factors governing the radiation conditions of the Earth's atmosphere. Study of radiation spectra gives an important information for calculation of radiation transfer in the atmosphere.[1,2]

In this paper we present the techniques for solar radiation measurements and data processing. A spectrophotometer designed to record the direct and scattering solar radiation in the spectral range from 400 to 700 nm is described. Besides, some measurement results obtained in 1996 are presented.

EQUIPMENT AND THE MEASUREMENT METHOD

The direct and scattered solar radiation was measured with the spectrophotometer built on the base of KSVU–23 automated spectral system. The latter consists of MDR–23 monochromator and a unit for control and data acquisition based on the DVK–2 minicomputer. The control unit consists of units, which control a monochromator stepper motor and voltage across PMT, as well as the data storage board with a 12-bit 20-kHz 6-channel ADC. FEU–100 PMT was used as a receiver. The radiation was recorded within the spectral range from 400 to 700 nm with the 1 nm resolution. The time of a single spectrum recording was 1 min. The information was stored in a magnetic carrier for further IBM PC processing. The solar radiation came into the monochromator through light guide *1* of 1 mm diameter (Fig. 1). One end of the light guide was attached to monochromator slit, while another one was placed behind the focal plane of the lens of receiving telescope *5* (when measuring the direct solar radiation) or directed onto diffusely scattering gypsum screen *2* or convex mirror *3* (at all-sky measurements). In the latter case, the contribution from the direct solar radiation was eliminated with shading screen *4*. The ratio of the total image area covered with design elements and the screen to the total area of the celestial hemisphere did not exceed 1.5%.

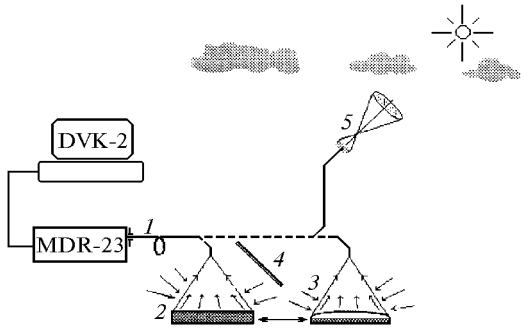

FIG. 1. Schematic diagram of the spectrophotometer.

The spectrophotometer was calibrated against the TRSh–2750 lamp with the known spectrum L_T. As a result, calibration curves were obtained for measurements by the direct solar radiation, diffusely scattering screen, and convex mirror (Fig. 2, right axis).

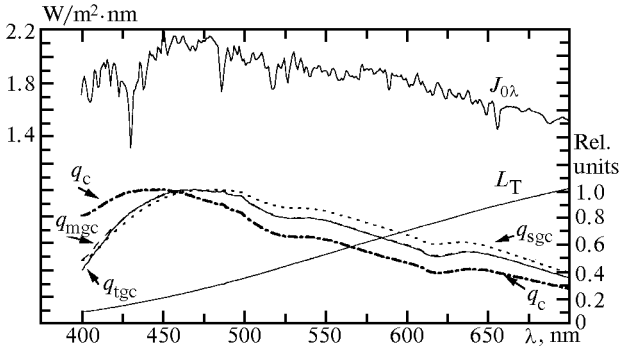

FIG. 2. $J_{0\lambda}$ is the extraterrestrial solar constant; the calibration curves are scaled to maximum; L_T is the theoretical curve of the TRSh–2750 lamp; q_c is the spectral sensitivity of the monochromator; q_{mgc}, q_{tgc}, and q_{sgc} are the spectral sensitivities of the paths: mirror – light guide – monochromator, telescope – light guide – monochromator, and screen – light guide – monochromator.

For standard cloud formations, the extinction coefficient in the visible spectral range changes

0235-6880/99/02 144-04 $02.00

sufficiently smoothly with the wavelength. Therefore, we smoothed out the initial signals by five points in order to decrease a random error. The final resolution was 5 nm. The following parameters were under analysis:

– spectral optical thickness per unit air mass;

– spectral flux of the solar radiation scattered by the sky and scaled to the extraterrestrial solar spectrum per unit air mass, in relative units.

In the general case, a recorded signal can be written as

$$U_\lambda(\theta) = C\, q_\lambda\, J_{0\lambda}\, T_{\lambda_a}(\theta)\, T_{\lambda_m}(\theta), \qquad (1)$$

where q is the constant estimated from the measurements; q_λ is the spectral sensitivity of the spectrophotometer; $J_{0\lambda}$ is the extraterrestrial solar constant[3] (see Fig. 2, left axis); $T_{\lambda_a}(\theta)$ is the spectral transmittance of the atmospheric aerosol at a solar zenith angle θ; $T_{\lambda_m}(\theta)$ is the spectral transmittance of the atmospheric air (molecular scattering and absorption) at a solar zenith angle θ:

$$T_{\lambda_a}(\theta) = \exp(-\tau_{\lambda_a}/\cos\theta),$$

$$T_{\lambda_m}(\theta) = \exp(-\tau_{\lambda_m}/\cos\theta), \qquad (2)$$

where τ_{λ_a} and τ_{λ_m} are the spectral optical density of aerosol and molecular air masses of the atmosphere (τ_{λ_m} can be determined by the Pendorf formula as $\tau_{\lambda_m} = 1.545 \cdot 10^{10} \cdot \lambda^{-4.086}$). Although weak bands of such gaseous atmospheric constituents as ozone, carbon dioxide, oxygen, and water vapor are present in the spectral range under study, their contribution into extinction is insignificant in comparison with the aerosol and molecular scattering.

For the case of direct solar radiation measurements, let us transform Eq. (1) to the form

$$U_\lambda(\theta)/q_\lambda J_{0\lambda} = U^0_\lambda(\theta) = C\, T_{\lambda_a}(\theta)\, T_{\lambda_m}(\theta). \qquad (3)$$

Having taken a logarithm of Eq. (3) for two solar zenith angles θ_1 and θ_2, we obtain:

$$\ln U^0_\lambda(\theta_1) = \ln C - \frac{\tau_{\lambda_a}}{\cos\theta_1} - \frac{\tau_{\lambda_m}}{\cos\theta_1}, \qquad (4)$$

$$\ln U^0_\lambda(\theta_2) = \ln C - \frac{\tau_{\lambda_a}}{\cos\theta_2} - \frac{\tau_{\lambda_m}}{\cos\theta_2}. \qquad (5)$$

Then Eqs. (4) and (5) are multiplied by $1/\cos\theta_2$ and $1/\cos\theta_1$, and Eq. (5) is subtracted from Eq. (4). Thus we obtain the equation for the constant q:

$$\frac{1}{\cos\theta_2}\ln\left[U^0_\lambda(\theta_1)\right] - \frac{1}{\cos\theta_1}\ln\left[U^0_\lambda(\theta_2)\right] = \left(\frac{1}{\cos\theta_2} - \frac{1}{\cos\theta_1}\right)\ln C. \qquad (6)$$

From Eq. (6) we can find

$$C = \exp\left\{\frac{\frac{1}{\cos\theta_2}\ln\left[U^0_\lambda(\theta_1)\right] - \frac{1}{\cos\theta_1}\ln\left[U^0_\lambda(\theta_2)\right]}{\frac{1}{\cos\theta_2} - \frac{1}{\cos\theta_1}}\right\}. \qquad (7)$$

Then from Eqs. (2) and (3) we have

$$\tau_{\lambda_a} = \ln C\, T_{\lambda_m}/U^0_\lambda. \qquad (8)$$

In measurements with the convex mirror, τ_{λ_a} was determined by Eq. (8). For the case of the diffuse screen we can obtain, by analogy,

$$\tau_{\lambda_a} = \cos\theta \ln\left[\frac{C\cos\theta\, T_{\lambda_m}(\theta)}{U^*_\lambda}\right], \qquad (9)$$

where $U^*_\lambda = \dfrac{U_{\lambda\Sigma} - F}{q_\lambda J_{0\lambda}}$, in which $U_{\lambda\Sigma}$ is the total (direct plus scattered) solar radiation flux, and F is the scattered solar radiation flux.

RESULTS OF MEASUREMENTS

During the measurement campaign of 1996 more than 200 solar radiation spectra were recorded in the spectral range from 400 to 700 nm. Among them, spectra of scattered solar radiation comprise more than 90%.

Figure 3 gives the results of reconstruction of the aerosol spectral optical thickness dated to October 8 of 1996 (from 02:00 a.m. till 06:00 p.m., local time), when measuring the direct solar radiation. The curves *1–4* were obtained at recording the direct solar radiation under clear sky conditions and through very thin cloud layers, the curves *5–8* were obtained at measurements through denser translucent clouds of the upper atmosphere. For comparison, the data on the optical thickness obtained from independent measurements with the stellar–solar spectrophotometer[4] at 01:58 p.m. under clear sky conditions are also shown in the figure (triangles).

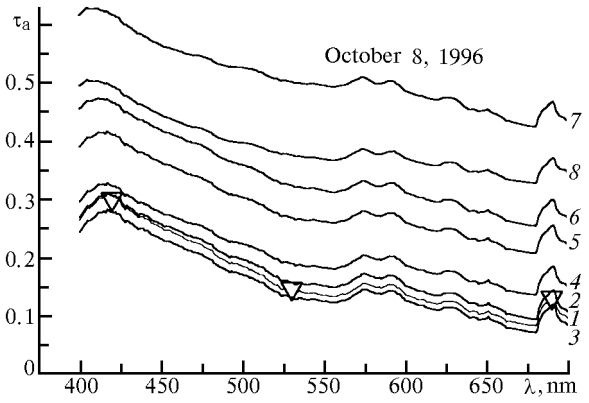

FIG. 3. Spectral optical thickness of aerosol.

Scattered solar radiation fluxes were measured with the help of the diffusely scattering gypsum screen. Figure 4 gives the characteristic curves of solar radiation flux obtained under clear sky (curve 8), lower dense overcast (the bottom family of

curves), and upper overcast (the top family of curves) conditions.

Typically, for radiation scattering in the air, the radiation flux monotonically decreases (curve *8*) as the wavelength increases. The ratio between the flux at the beginning of the spectral range (400 nm) and at its end (700 nm) is from 2.5 to 2.7. The curve is not quite smooth. Minima near 465, 550, 580, and 680 nm are noticeable, as well as a dip between 550 and 650 nm. As to curves *1–5* (see Fig. 4) describing the radiation scattering by overcast translucent clouds, they demonstrate the spectral structure similar to that observed under cloudless conditions (curve *8*). However, in contrast to the latter, this spectral structure is more pronounced, and its amplitude is several times greater, although the relative amplitudes are practically the same. A trend of monotonic decrease of spectral flux is practically absent in these curves. A neutral behavior of the spectral curves is especially marked in cases of lower, overcast, and dense cloudiness (curves *9*, *10*, and *11* in Fig. 4). The spectral structure is almost fully blurred in this case. Different spectral behavior of curves *2*, *4*, *6*, and *7* corresponding to one type of clouds can likely be explained by their different optical thickness, which was not under monitoring in that experiment.

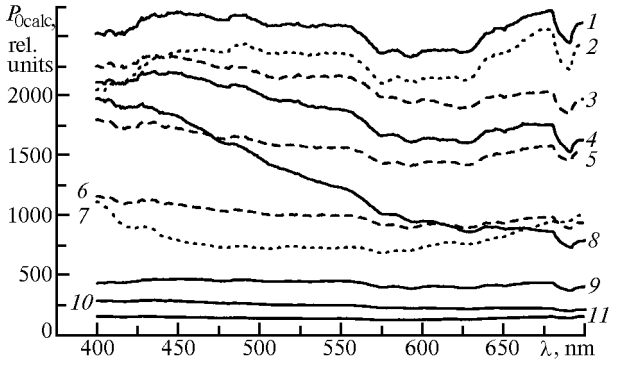

FIG. 4. Solar radiation flux under overcast conditions: 10/Cs fib, dense haze (1); 10/Sc trans (2); 9/Ac und (3); 10/Sc (4); 10/Ac floc, Ac und 6–7 (5); 10/Sc trans (6); 10/Sc op (7); cloudless conditions (8); 10/Sc, St (9); 10/St (10); 10/Sc und (11).

The curves of the spectral flux for the case of broken clouds (the cloud fraction index is up to 6) are shown in Fig. 5. A decrease in the spectral flux with increasing wavelength is typical for them, as in the case of the clear sky (curve *5*). However, it is less pronounced. Spectral structure, as for the curves shown in Fig. 4, is clearly seen here. Coming back to Fig. 3, we can see that oscillations of all curves are in antiphase with oscillations of the spectral flux curves shown in Figs. 4 and 5. This means that the observed maxima are caused by absorption of the radiation by atmospheric gases. A peak at 690 nm is especially pronounced. It corresponds to absorption bands of oxygen and water vapor.[5]

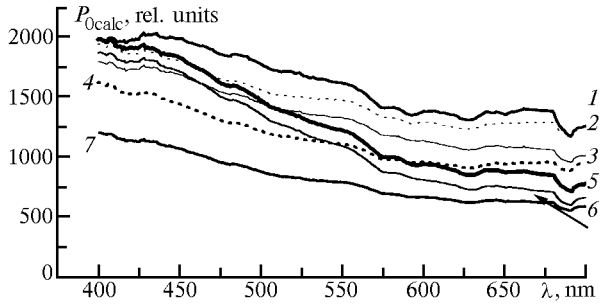

FIG. 5. Solar radiation flux under broken cloudiness conditions: 0–1/Cs (1); 2/Ci fib – 6/Cu hum (2); 6/Cu hum, med (3); 3/Ac und (4); clear sky (5); 2/Ci – 2/Ac cuf (6); 2/Ac cuf, haze (7).

A tentative analysis of the obtained array of data on the scattered solar radiation fluxes has shown an applicability of the method of linear regression within the entire spectral range from 400 to 700 nm. Since most curves have a distinct inflection near 575 nm, the entire spectral region was divided into two subregions. Tangent of an angle of curve slope is shown in Fig. 6 as a function of the cloud amount index for the two spectral subregions: from 400 to 575 and from 575 to 700 nm. Straight lines in the figure denote the result of linear regression analysis for these two subarrays obtained. For the top straight line the tangent is equal to 0.28 ± 0.042, while for the lower one it is 0.404 ± 0.047.

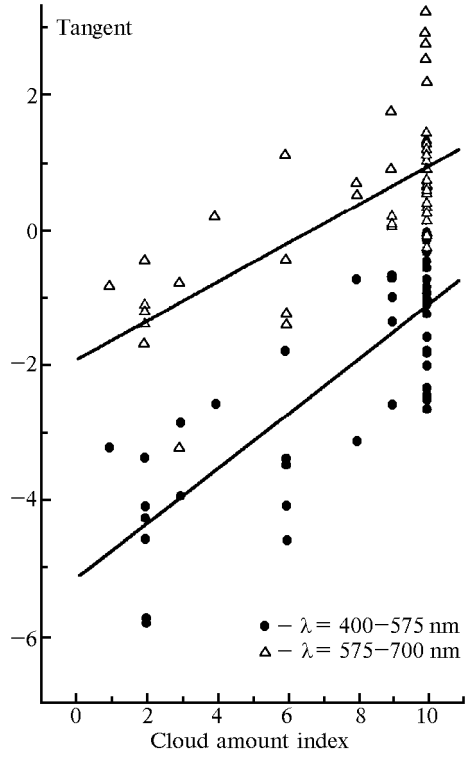

FIG. 6. Tangent of the slope angle for curves of solar radiation flux vs. the cloud amount index for the spectral regions from 400 to 575 (circles) and from 575 to 700 nm (triangles).

From the analysis of the data obtained, the following conclusions can be made:

1) under conditions of broken clouds and clear sky, the spectral flux monotonically decreases due to aerosol extinction and molecular scattering of solar radiation;

2) the spectral flux structure under the overcast translucent cloudiness and clear sky conditions is formed due to molecular absorption of solar radiation;

3) under the conditions of low overcast and dense cloudiness, the spectral flux behaves neutrally. In this case it is determined by scattering by clouds; spectral structure of solar radiation flux is blurred;

4) the slope of curves depends more strongly on the cloud amount index in the range from 400 to 575 nm than in the range from 575 to 700 nm.

ACKNOWLEDGMENT

This work was done at the Siberian Lidar Station under partial financial support of the Russian Ministry of Science (Project No. 01–64).

REFERENCES

1. R.M. Goody, *Atmospheric Radiation* [Russian translation] (Mir, Moscow, 1966), 522 pp.
2. Yu. Ross, et al., *Cloudiness and Radiation* (Tartu, 1975), 251 pp.
3. J.C. Arvesen, et al., Appl. Optics **8**, No. 11, 2215–2232 (1969).
4. A.I. Abramochkin, V.P. Galileiskii, et al., in: *Measurements of Optical and Meteorological Parameters of the Atmosphere with Use of Laser Radiation* (Institute of Atmospheric Optics of the Siberian Branch of the Academy of Sciences of the USSR, Tomsk, 1981), pp. 14–19.
5. V.I. Binenko and K.Ya. Kondrat'ev, Tr. Gl. Geofiz. Obs., issue 331, 3–17 (1975).